Table 2 Clinical, biochemical and genetic characteristics of families with variegate porphyria and hereditary coproporphyria

Fam	Pts	Sex	Age/age at first symptom	Gene	Nucleotide change	Amino acid change	Symptoms		Plasma scan	Urine					Feces					
							Acute	Skin		PBG	ALA	TPu	Uro	Cop	TPf	Uro	Cop	Proto	TF	TT
I-VP	P1	F	28/21	PPOX	c.441-442delCA	Frame-shift	+	–	626	37	40	4,675	2,340	2,335	–	–	–	–	Inf + M	Glu
	D	F	11	PPOX	c.441-442delCA	Frame-shift	–	–	ND	–	–		–	–	–	–	–	–	–	–
II-VP	P2	F	30/24	PPOX	c.917T>C	p.L306P	+	+	626	383		7,076	–	–	2,422[a]	–	–	–	Inf + M	Glu
	So	M	3	PPOX	c.917T>C	p.L306P	–	–	Neg	2	13	0	–	–	0.6	–	–	–	–	–
III-VP	P3	M	69/39	PPOX	c.917T>C	p.L306P	–	+	626	3	19	1,326	143	1,183	671	84	241	346		Ph
	So	M	43/30	PPOX	c.917T>C	p.L306P	+	+	627	75	223	930	–	–	1,753	–	–	–	–	Glu
	G	M	10	PPOX	Neg	–	–	–	Neg	3	15	120	–	–	138	–	–	–	–	–
IV-VP	P4	F	80/45	PPOX	c.917T>C	p.L306P	–	+	626	2.2	16.8	1,340	79	1,261	3,182	890	662	1,630	–	Ph
	D	F	58	PPOX	c.917T>C	p.L306P	–	+	626	3.7	30	199[a]	–	–	1,202[a]	–	–	–	–	–
	So	M	48	PPOX	c.917T>C	p.L306P	–	–	Neg	5	32	0	–	–	142	–	–	–	–	–
V-VP	P5	F	31/25	PPOX	c.1252T>C	p.C418R	+	+	626	505	309	14,326	–	–	–	–	–	–	Inf + M	
	Si	F	38/25	PPOX	c.1252T>C	p.C418R	+	+	626	11[a]	33[a]	217[a]	–	–	–	–	–	–	Inf	
	So	M	19	PPOX	Neg	–	–	–	Neg	7	29	68	–	–	–	–	–	–	–	
	Ni	F	16	PPOX	c.1252T>C	p.C418R	–	–	ND	–	–		–	–	–	–	–	–	–	
	Nf	M	17	PPOX	Neg	–	–	–	ND	–	–		–	–	–	–	–	–	–	
VI-VP	P6	M	63/35	PPOX	c.1252T>C	p.C418R	–	+	626	8	66	626	74	552	268	3	88	177	–	
I-HCP	P	F	22/22	CPOX	c.364G>T	p.E122X	+	–	618	53	63	5,100	1,425	4,100	4,960	–	–	–	Inf + M	Glu

Fam, family, *Pts* patients, *P* proband number, *Si* sister, *D* daughter, *Ni* niece, *Nf* nephew, *G* grandson, *F* female, *M* male, *PBG* porphobilinogen, normal value: <15 μmol/24 h, *ALA* δ-aminolevulinic acid, normal range: 11.4–57.2 μmol/24 h, *TPu* total porphyrins in urine, normal values <200 nmol/24 h, *Plasma scan* plasma fluorescence emission peak in nm, *TPf* total porphyrins in feces, normal values <150 nmol/g dry weight, *Uro* uroporphyrin, normal values: <36 nmol/24 h in urine, <1 nmol/g dry weight in feces, *Cop* coproporphyrins, normal values: <122 nmol/24 h in urine, <26 nmol/g dry weight in feces, *Proto*, protoporphyrins, normal value: <80 nmol/g dry weight in feces, *TF* triggering factor, *Inf* infection, *M* medication, *TT* treatment, *Glu* 10% glucose i.v. infusion, *Ph* photoprotection, *ND* not determined, *Neg* no emission peak on plasma scan

[a] Mark, values measured after resolution of the acute attack

onset, with a frequency similar to that reported in South Africa and Western Europe (Whatley et al. 1999). The patient with HCP manifested with acute symptoms only. During onset, all of the patients had markedly increased levels of PBG and ALA. In all of the investigated AIP probands, except for one (family VI-P6), the HMBS activity in the erythrocytes was decreased. In P6, the HMBS activity was measured during acute onset, when transitory normal levels could be expected. Heme-arginate is not available in Bulgaria; therefore, all patients with acute onset, except for one, were treated with i.v. glucose infusions (from 200 to 500 g/day according to the severity of the attack) or Cimetidine until the clinical and biochemical parameters improved.

A total of six different mutations in HMBS were detected in all seven families with AIP, three of which were previously described as single nucleotide substitutions: c.76C > T [p.R26C] in exon 3, c.287C > T [p.S96F] in exon 7, and c.445C > T [p.R149X] in exon 9; the other three mutations were newly detected. The novel ones included a single nucleotide change, a small insertion and a single nucleotide deletion: c.345-2A > C in intron 7–8, c.279-280insAT in exon 7, and c.887delC in exon 15. Overall, there were two missense, one nonsense, one splice-site, and two frameshift mutations. The alterations identified in the Bulgarian patients were heterogeneous, as previously reported in many other populations (Whatley et al. 2009; Puy et al. 1997).

Three of the substitutions identified in the Bulgarian AIP patients have been reported in various ethnic populations. The mutations identified in families I-P1 (p.R26C) and IV-P4 (p.R149X) were initially identified in Finish patients (Kauppinen et al. 1995). p.R26C has been subsequently reported in Slavic (Hrdinka et al. 2006), Spanish (To-Figueras et al. 2006), French (Puy et al. 1997), Chinese (Yang et al. 2008), and Venezuelan populations (Paradisi and Arias 2010). The p.R149X mutation was found to be one of the relatively prevalent mutations (approximately 5%) in a large cohort of 109 mutation-positive AIP families (Puy et al. 1997). It has been shown that the R26 and R149 residues are located in the substrate-binding site and are crucial for enzymatic activity (Llewellyn et al. 1998; Gill et al. 2009). AIP family IV is of particular interest due to its gypsy origin. The gypsy people represent the largest minority in Bulgaria, and the search for the p.R149X substitution in this population deserves further attention.

In families VI-P6 and VII-P7, an identical p.S96F missense mutation was found in the HMBS gene; this mutation was first described by Kaupinnen et al. (2002). There was no significant difference in the clinical phenotype of the two probands; both patients presented with a single acute attack that was triggered by hormonal changes during their twenties. At present, both patients are symptom-free.

Novel substitutions in the HMBS gene that resulted in frameshift and splice-site alterations were identified in families II, III, and V. A small insertion (c.279-280insAT in exon 7) was identified in the II-P2 proband, resulting in a frameshift mutation that led to the formation of premature stop codon after the incorporation of 24 different amino acid residues, compared to the reference transcript. A small out-of-frame deletion (c.887delC) was identified in the III-P3 family, and this mutation led to a premature stop codon after 3 amino acids, compared to the reference sequence. The nucleotide change revealed in family V-P5 (c.345-2A>C in intron 7) affected the invariant AG acceptor splice site and possibly interfered with mRNA processing. At the same position, a different nucleotide change (c.345-2 A>G) has been reported in Swedish patients, listed in a table (Floderus et al. 2002). These three alterations have not been reported in reference databases (such as dbSNP, HGMD, 1KG, and ESP). To exclude the possibility of the novel mutations being SNPs, 96 control DNA samples were screened, and no samples revealed the presence of the novel mutations of the HMBS gene (c.345-2A>C in intron 7, c.279-280insAT in exon 7, and c.887delC in exon 15). The above finding suggests that these mutations are pathogenic. RNA analysis is needed to prove the pathogenicity of the c.345-2A > C change.

After detecting specific mutations in the families, the available family members ($n = 4$ symptomatic and $n = 5$ asymptomatic) were screened for the presence of the identified mutations (Table 1). All symptomatic relatives harbored the corresponding family-specific nucleotide changes. Among the five asymptomatic subjects three were mutation positive, including family II-M, VI-D, and VII-D subjects. Subject II-M was a postmenopausal female with a low level of HMBS activity in the erythrocytes and concomitant diabetes mellitus type II. Even if the diabetes has been treated, a slightly elevated serum glucose levels could exert a protective effect against overt disease (Andersson and Lithner 2001). Subjects VI-D and VII-D, females presently aged 21 and 15 years, respectively, whose HMBS activity levels in the erythrocytes were unavailable, shared identical causative mutations, which facilitated genetic counseling to prevent acute attacks. The HMBS levels in the four mutation negative subjects were within the normal range in two cases and were unavailable in the other two cases.

A total of three different novel substitutions in the PPOX gene were found in all six families with VP: c.441-442delCA in exon 5, c.917T>C [p.L306P] in exon 9, and c.1252T>C [p.C418R] in exon 12. In total, two missense mutations and one small deletion were observed in the VP families. All of the probands from families I, II, III, IV, V, and VI had positive plasma scan at 626 nm, increased levels of urinary porphyrins and their precursors PBG and

ALA. Probands from families II, III, IV, and VI had increased fecal porphyrins levels as well. A small out-of-frame deletion (c.441-442delCA) was found in family I-P1; this mutation led to a premature stop codon after the introduction of nine different amino acids. Families II-P2, III-P3, and IV-P4 shared an identical mutation (c.917T>C) that resulted in a leucine to proline substitution at position 306 (p.L306P). The V-P5 and VI-P6 probands harbored an identical change (c.1252T>C) that led to the replacement of a cysteine with proline in codon 418 (p.C418R). These three novel alterations have not been reported in reference databases (such as dbSNP, HGMD, 1KG, and ESP) and were not detected in the 96 control DNA samples. Residues L306 and C418 are located in the highly conserved FAD-binding domain (Qin et al. 2011), and these alterations most likely disrupt this interaction. The HumVar scores of 1.00 for p.L306P and 0.921 for p.C418R predicted that these mutations are most likely damaging. A small deletion (c.916_917delCT) in codon 306 has been described by Wiman et al. (2003), while no mutations have been reported in codon 418 so far. The available family members ($n = 3$ symptomatic and $n = 7$ asymptomatic) were screened for the presence of the corresponding nucleotide changes, and the details of these individuals are shown in Table 2. The symptomatic subjects III-So, IV-D, and V-Si harbored the family-specific nucleotide changes. Family III-So had an acute attack followed by chronic neurological symptoms and skin involvement and increased levels of PBG, ALA, total porphyrins in urine and feces. Family IV-D suffered from cutaneous lesions only. She had a plasma emission peak at 626 nm, normal PBG and ALA levels due to the lack of acute symptoms, and increased levels of urinary and fecal porphyrins. Family V-Si suffered from acute onset and cutaneous legions, unfortunately PBG and ALA levels shown in Table 2 were measured after the acute onset and were within normal range. However, plasma emission peak at 626 nm and increased total porphyrins in urine were observed even after the resolution of the attack. Among the seven asymptomatic subjects, four harbored the specific alterations, family I-D, II-So, IV-So, and V-Ni. Unfortunately, no biochemical data was available for the adolescent individuals I-D and V-Ni. Family II-So and IV-So had normal total porphyrins levels in urine and feces and urinary PBG and ALA levels. Plasma scan was also negative in both subjects. These results could be expected considering the fact that the significance of plasma emission peak at 626 nm is partly limited in the elderly asymptomatic carriers (IV-So). It is usually absent in asymptomatic children (II-So) (Hift et al. 2004). Unfortunately, PPOX activity could not be measured to check the cosegregation of the mutation and low enzymatic activity levels. Further analysis is needed to prove the pathogenicity of these alterations.

The majority of Bulgarian VP patients can be associated with 2 endemic regions. One of these regions is populated with ethnic Bulgarians, who are Muslim. These individuals reside in remote villages around the mountain town of Velingrad in the Rhodope mountains. Only 2 families, V and VI, from this region agreed to take part in this study, although more patients were invited. Most likely, the majority of VP patients share the identical p.C418R mutation due to consanguinity. The ancestors of families II, III, and IV originated from the small remote village of Buynovtsi, which is situated in the central Balkan mountains. Thus, a possible founder effect can also be anticipated for the p.L306P change. The endemic aggregation of families with VP and the distribution of the corresponding novel missense mutation also emphasize the pathogenic effect of these novel alterations.

A novel nonsense mutation (c.364G>T [p.E122X]) was identified in the patient with HCP shortly after her first acute attack in 2013; the details of this patient can be found in Table 2. She had increased total porphyrins levels in urine and feces and urinary PBG and ALA. Plasma scan emission peak was at 618 nm. Cutaneous involvement was absent. The p.E122X mutation is located in exon 1 and would lead to an unstable and inactive CPOX protein, which is likely removed by proteolytic degradation. The CPOX activity measurements could not be performed to prove the cosegregation of the novel alteration and low enzymatic activity.

This is the first report to describe mutations in Bulgarian patients with AIP, VP, and HCP. We identified a total of seven novel mutations in these families. Seven latent gene carriers were also detected. The identification of the latent gene carriers can result in the prevention of acute attacks by avoiding the well-known exogenic triggering factors.

Acknowledgements We would like to thank all of the families that participated in this study. We would also like to gratefully acknowledge Prof. Dimcho Adjarov for the fruitful discussions and suggestions, as well as for supplying the clinical and biochemical data used in this study. Mrs. Doroteya Leonkeva, Mrs. Kumi Kato, and Ms. Yoko Tateda are also gratefully acknowledged for their skillful technical assistance. We acknowledge the support from Ministry of Education, Culture, Sports, Science, and Technology of Japan (MEXT)

Take-Home Message

This is the first report to describe mutations in Bulgarian patients with acute hepatic porphyrias, and a total of seven novel mutations were identified in this study.

References to Electronic Databases

MIM 176000; OMIM 176200; OMIM 121300; EC 4.3.1.8; EC 1.3.3.4; EC 1.3.3.3; HMBS; PPOX; CPOX; HMBS Ensembl Accession number ENST00000442944; PPOX Ensembl Accession number ENST00000367999; CPOX Ensembl Accession number ENST00000264193; www.hgmd.cf.ac.uk

Compliance with Ethics Guidelines

Conflict of Interest

Sonya Dragneva, Monika Szyszka-Niagolov, Aneta Ivanova, Lyudmila Mateva, Rumiko Izumi, Yoko Aoki, and Yoichi Matsubara declare that they have no conflicts of interest.

Informed Consent

All procedures followed were in accordance with the ethical standards of the responsible committee on human experimentation (institutional and national) and with the Helsinki Declaration of 1975, as revised in 2000 (5). Informed consent was obtained from all patients for being included in the study.

Details of the Contribution of Individual Authors

Sonya Dragneva: involved in design, analysis, and interpretation of data, drafted the initial version of the manuscript; Monika Niagolov: involved in conception and design and critical revision of the manuscript; Aneta Ivanova: involved in conception, design, and critical revision of the manuscript; Lyudmila Mateva: involved in conception, design, and critical revision the manuscript; Rumiko Izumi: involved in analysis and interpretation of data and critical revision of the manuscript; Yoko Aoki: involved analysis and interpretation of data and critical revision of the manuscript; Yoichi Matsubara (Guarantor): involved in analysis and interpretation of data and critical revision of the manuscript

References

Adjarov DG, Naydenova EN, Kerimova MA, Pentieva ED, Ivanova LB, Ivanova VA (1994) Influence of protein calorie malnutrition and fasting on the activities of δ-aminolevulinic acid dehydratase and porphobilinogen deaminase in rats. Exp Toxicol Pathol 46:199–202

Andersson C, Lithner F (2001) Diabetic metabolism protective in severe acute intermittent porphyria. Lakartidningen 98 (51–52):5874–5876

Barbaro M, Kotajarvi M, Harper P, Floderus Y (2013) Partial protoporphyrinogen oxidase (PPOX) gene deletions, due to different Alu-mediated mechanisms, identified by MLPA analysis in patients with variegate porphyria. Orphanet J Rare Dis 8:13

Deacon AC, Elder GH (2001) Front line tests for the investigation of suspected porphyria. ACP Best Practice No 165. J Clin Pathol 54:500–507

Deybach JC, de Verneuil H, Nordmann Y (1981) The inherited enzymatic defect in porphyria variegata. Hum Genet 58 (4):425–428

Floderus Y, Shoolingin-Jordan PM, Harper P (2002) Acute intermittent porphyria in Sweden. Molecular, functional and clinical consequences of some new mutations found in the porphobilinogen deaminase gene. Clin Genet 62(4):288–297

Gill R, Kolstoe S, Mohammed F et al (2009) Structure of human porphobilinogen deaminase at 2.8 A: the molecular basis of acute intermittent porphyria. Biochem J 420(1):17–25

Hift RJ, Davidson BP, van der Hooft C, Meissner DM, Meissner PN (2004) Plasma fluorescence scanning and fecal porphyrin analysis for the diagnosis of variegate poprhyria: precise determination of sensitivity and specificity with detection of protoporphyrinogen oxidase mutations as a reference standard. Clin Chem 50(5):915–923

Hrdinka M, Puy H, Martasek P (2006) Update in porphobilinogen deaminase gene polymorphisms and mutations causing acute intermittent porphyria: comparison with the situation in Slavic population. Physiol Res 55(2):S119–S136

Kappas A, Sassa S, Galbraith RA, Nordmann Y (1995) The porphyrias. In: Scriver CR, Beaudet AL, Sly WS, Valle D (eds) Metabolic and molecular bases of inherited disease, 7th edn. McGraw-Hill, New York, vol 2, pp 2103–2159

Kauppinen R, Mustajoki S, Pihlaja H, Peltonen L, Mustajoki P (1995) Acute intermittent porphyria in Finland: 19 mutations in the porphobilinogen deaminase gene. Hum Mol Genet 4(2):215–222

Kaupinnen R, von und zu Fraunberg M (2002) Molecular and biochemical studies of acute intermittent porphyria in 196 patients and their families. Clin Chem 48(11):1891–1900

Llewellyn DH, Whatley S, Elder GH (1998) Acute intermittent porphyria caused by an arginine to histidine substitution (R26H) in the cofactor-binding cleft of porphobilinogen deaminase. Hum Mol Genet 2(8):1315–1316

Lockwood WH, Poulos V, Rossi E, Curnow DH (1985) Rapid procedure for fecal porphyrin assay. Clin Chem Jul 31 (7):1163–1167

Mauzarell D, Granick S (1956) The occurrence and determination of δ-amino-levulinic acid and porphobilinogen in urine. J Biol Chem 219(1):435–446

Meissner PN, Dailey TA, HIft RJ, Ziman M, Corrigal AV, Roberts AG et al (1996) A R59W mutation in human protoporphyrinogen oxidase results in decreased enzyme activity and is prevalent in South Africans with variegate porphyria. Nat Genet 13(1):95–97

Meyer UA, Strand LJ, Doss M, Rees AC, Marver HS (1972) Intermittent acute porphyria – demonstration of a genetic defect in porphobilinogen metabolism. N Engl J Med 286 (24):1277–1282

Mustajoki P (1981) Normal erythrocyte uroporphyrinogen I synthase in a kindred with acute intermittent porphyria. Ann Intern Med 95(2):162–166

Paradisi I, Arias S (2010) Marked geographic aggregation of acute intermittent porphyria families carrying mutation Q180X in Venezuelan populations, with description of further mutations. J Inherit Metab Dis. doi:10.1007/s10545-010-9228-x

Puy H, Deybach JC, Lamoril J et al (1997) Molecular epidemiology and diagnosis of PBG deaminase gene defects in acute intermittent porphyria. Am J Hum Genet 60(6):1373–1383

Qin X, Tan Y, Wang L et al (2011) Structural insight into human variegate porphyria disease. FASEB J 25:653–664

Rimington C (1971) Quantitative determination of porphobilinogen and porphyrins in urine and porphyrins in faeces and erythrocytes. Assoc Clin Pathol Broadsheet 70:1–9

Sassa S (2006) Modern diagnosis and management of the porphyrias. Br J Haematol 135(3):281–292

Thunnel S, Floderus Y, Henrichson A, Harper P (2006) Porphyria in Sweden. Physiol Res 55(Suppl 2):S109–S118

To-Figueras J, Badenas C, Carrera C et al (2006) Genetic and biochemical characterization of 16 acute intermittent porphyria cases with a high prevalence of R173W mutation. J Inherit Metab Dis 29(4):580–585

Whatley SD, Puy H, Morgan R et al (1999) Variegate porphyria in Western Europe: identification of PPOX gene mutations in 104 families, extent of allelic heterogeneity, and absence of correlation between phenotype and type of mutation. Am J Hum Genet 65(4):984–994

Whatley SD, Mason NG, Woolf JR, Newcombe RG, Elder GH, Badminton MN (2009) Diagnostic strategies for autosomal dominant acute porphyrias: retrospective analysis of 467 unrelated patients referred for mutational analysis of the HMBS, CPOX, or PPOX gene. Clin Chem 55(7):1406–1414

Wiman A, Harper P, Floderus Y (2003) Nine novel mutations in the protoporphyrinogen oxidase gene in Swedish families with variegate porphyria. Clin Genet 64(2):122–130

Yang CC, Kuo HC, You HL et al (2008) HMBS mutations in Chinese patients with acute intermittent porphyria. Ann Hum Genet 72 (Pt 5):683–686

OPEN ACCESS Freely available online

PLOS | ONE

TBX1 Mutation Identified by Exome Sequencing in a Japanese Family with 22q11.2 Deletion Syndrome-Like Craniofacial Features and Hypocalcemia

Tsutomu Ogata[1*☯], Tetsuya Niihori[2☯], Noriko Tanaka[3☯], Masahiko Kawai[4], Takeshi Nagashima[5], Ryo Funayama[5], Keiko Nakayama[5], Shinichi Nakashima[1], Fumiko Kato[1], Maki Fukami[6], Yoko Aoki[2], Yoichi Matsubara[2,6]

1 Department of Pediatrics, Hamamatsu University School of Medicine, Hamamatsu, Japan, **2** Department of Medical Genetics, Tohoku University School of Medicine, Sendai, Japan, **3** Department of Pediatrics, Kurashiki Central Hospital, Kurashiki, Japan, **4** Department of Pediatrics, Kyoto University School of Medicine, Kyoto, Japan, **5** Division of Cell Proliferation, United Centers for Advanced Research and Translational Medicine, Tohoku University Graduate School of Medicine, Sendai, Japan, **6** National Research Institute for Child Health and Development, Tokyo, Japan

Abstract

Background: Although *TBX1* mutations have been identified in patients with 22q11.2 deletion syndrome (22q11.2DS)-like phenotypes including characteristic craniofacial features, cardiovascular anomalies, hypoparathyroidism, and thymic hypoplasia, the frequency of *TBX1* mutations remains rare in deletion-negative patients. Thus, it would be reasonable to perform a comprehensive genetic analysis in deletion-negative patients with 22q11.2DS-like phenotypes.

Methodology/Principal Findings: We studied three subjects with craniofacial features and hypocalcemia (group 1), two subjects with craniofacial features alone (group 2), and three subjects with normal phenotype within a single Japanese family. Fluorescence *in situ* hybridization analysis excluded chromosome 22q11.2 deletion, and genomewide array comparative genomic hybridization analysis revealed no copy number change specific to group 1 or groups 1+2. However, exome sequencing identified a heterozygous *TBX1* frameshift mutation (c.1253delA, p.Y418fsX459) specific to groups 1+2, as well as six missense variants and two in-frame microdeletions specific to groups 1+2 and two missense variants specific to group 1. The *TBX1* mutation resided at exon 9C and was predicted to produce a non-functional truncated protein missing the nuclear localization signal and most of the transactivation domain.

Conclusions/Significance: Clinical features in groups 1+2 are well explained by the *TBX1* mutation, while the clinical effects of the remaining variants are largely unknown. Thus, the results exemplify the usefulness of exome sequencing in the identification of disease-causing mutations in familial disorders. Furthermore, the results, in conjunction with the previous data, imply that *TBX1* isoform C is the biologically essential variant and that *TBX1* mutations are associated with a wide phenotypic spectrum, including most of 22q11.2DS phenotypes.

Citation: Ogata T, Niihori T, Tanaka N, Kawai M, Nagashima T, et al. (2014) *TBX1* Mutation Identified by Exome Sequencing in a Japanese Family with 22q11.2 Deletion Syndrome-Like Craniofacial Features and Hypocalcemia. PLoS ONE 9(3): e91598. doi:10.1371/journal.pone.0091598

Editor: Reiner Albert Veitia, Institut Jacques Monod, France

Received November 12, 2013; **Accepted** February 12, 2014; **Published** March 17, 2014

Funding: This work was supported in part by grants from the Ministry of Health, Labor, and Welfare, from the Ministry of Education, Culture, Sports, Science and Technology, and from the National Center for Child Health and Development. The funders had no role in study design, data collection and analysis, decision to publish, or preparation of the manuscript.

Competing Interests: The authors have declared that no competing interests exist.

* E-mail: tomogata@hama-med.ac.jp

☯ These authors contributed equally to this work.

Introduction

Chromosome 22q11.2 deletion syndrome (22q11.2DS) is a developmental disorder associated with characteristic craniofacial features with velopharyngeal incompetence, cardiovascular anomalies primarily affecting the outflow tracts, hypoparathyroidism and resultant hypocalcemia, and thymic hypoplasia leading to susceptibility to infection [1]. This condition is also frequently accompanied by non-specific clinical features such as developmental retardation [1]. Expressivity and penetrance of these features are highly variable and, consistent with this, chromosome 22q11.2 deletions have been identified in DiGeorge syndrome (DGS) and velocardiofacial syndrome (VCFS) with overlapping but different patterns of clinical features [1].

While multiple genes are involved in chromosome 22q11.2 deletions [2], *TBX1* (T-box 1) has been regarded as the major gene relevant to the development of clinical features in 22q11.2DS [3]. Indeed, heterozygous *TBX1* mutations have been identified in several deletion-negative patients with 22q11.2DS phenotype [2–8], and mouse studies argue for the critical role of *Tbx1* in the development of 22q11.2DS phenotypes [3]. However, the frequency of *TBX1* mutations remains rare in deletion-negative patients: Gong et al. identified only a few probable *TBX1* mutations after studying 40 patients with DGS/VCFS phenotypes

[4], and Zweier et al. found a single *TBX1* mutation after examining 10 patients with 22q11.2DS phenotype [8]. This indicates the presence of genetic heterogeneity in the development of 22q11.2DS phenotype in deletion-negative patients. Consistent with this, another DGS/VCFS locus has been assigned to chromosome 10p13-14 region [9]. Thus, it would be reasonable to perform a comprehensive genetic analysis in deletion-negative patients with 22q11.2DS phenotype.

In this regard, recent advance in molecular technologies has enabled to perform comprehensive genetic analyses, thereby contributing to the identification of underlying factors in genetic disorders. Indeed, genomewide array comparative genomic hybridization (CGH) has identified multiple disease-associated copy-number changes [10], and exome sequencing has discovered multiple disease-causing gene mutations [11]. In particular, these technologies can be powerful methods for familial disorders, because it is predicted that a single copy-number change or mutation is shared in common by affected subjects and is absent from non-affected subjects within a family.

Here, we performed array CGH analysis and exome sequencing in a family with 22q11.2DS-like clinical features. Although this study did not discover a novel disease gene, a *TBX1* mutation was successfully identified.

Materials and Methods

Ethics statement

The Institutional Review Board Committees of Hamamatsu University School of Medicine, Tohoku University School of Medicine, Kurashiki Central Hospital, and National Research Institute for Child Health and Development considered and approved the study, consent/assent procedures, and the publication of images and case details associated with this work. The individuals in this manuscript have given written informed consent (as outlined in PLOS consent form) to publish these case details. Actually, this study was performed after obtaining written informed consent from the parents of the child subjects and from the adult subjects. Furthermore, the mother and the elder brother aged 19 years old have given written informed consent to publication of the facial photographs of the two brothers; in addition, the younger brother aged 10 years has given informed assent.

Clinical Report

The pedigree of this Japanese family is shown in Fig. 1, and clinical findings of the family members are summarized in Table 1. The proband (subject III-5) was found to have hypocalcemia and hyperphosphatemia in a pre-operation laboratory test for repeated otitis media at 8 years of age, and was referred to Department of Pediatrics at Kurashiki Central Hospital. Subsequent examination revealed borderline low serum intact PTH value. Thus, he was diagnosed as having hypoparathyroidism, and received vitamin D therapy. Furthermore, physical examination showed characteristic craniofacial features with velopharyngeal incompetence suggestive of 22q11.2DS.

Similar craniofacial features were also exhibited by subjects II-2, III-1, III-6, and III-7, and hypocalcemia was also identified in subjects II-2 and III-7. Actually, subject II-2 was taking vitamin D, and subject III-7 was noticed to have hypocalcemia at birth because of the history of subject III-5, and was treated with vitamin D. The five subjects with 22q11.2DS-like craniofacial features lacked cardiovascular anomalies; while they also lacked susceptibility to infection, except for repeated otitis media in subject III-5, thymic hypoplasia was not evaluated in four of the five subjects. By contrast, the five subjects exhibited borderline to mild developmental delay. Indeed, adult subjects II-2 and III-1 had some difficulty in verbal communications, although they were able to get on their daily life, and subject II-2 was able to take care of family members. Similarly, child subjects III-5, III-6, and III-7 also showed speech delay, and subjects III-5 and III-7 received speech therapy. Furthermore, subject III-7 was diagnosed as having pervasive developmental disorder, and his verbal, performance, and full scale intelligence quotients were assessed as 63, 64, and 60, respectively, by the WISC-III method at 10 years of age. In addition, subject II-2 had sensorineural deafness, and subject III-5 had Graves' disease.

Molecularly Studied Subjects

Molecular studies were performed for eight subjects in this family, using peripheral blood samples. They were divided into three groups in terms of clinical findings: group 1, subjects II-2, III-5, and III-7 with craniofacial features and hypocalcemia; group 2, subjects III-1 and III-6 with craniofacial features alone; and group 3, subjects II-1, III-3, and IV-1 with apparently normal phenotype (Fig. 1).

FISH and Array CGH Analyses

Fluorescence *in situ* hybridization (FISH) analysis was performed with a probe for *HIRA* on the commonly deleted chromosome 22q11.2 region and that for *ARSA* at chromosome 22q13 utilized as an internal control (Abott). Array CGH was carried out using a genomewide 2x400K Agilent platform catalog array, according to the manufacturer's instructions (Agilent Technologies), and copy number variants/polymorphisms were screened with Agilent Genomic Workbench software using the Database of Genomic Variants (http://dgv.tcag.ca/dgv/app/home).

Exome and Sanger Sequencings

Exon capture was performed with the SureSelect Human All Exon kit v4 (Agilent Technologies). Exon libraries were sequenced with the Illumina Hiseq 2000 platform according to the manufacturer's instructions (Illumina), providing 108–122 average depth for each sample. Paired 101-base pair reads were aligned to the reference human genome (UCSChg19) using the Burrows-Wheeler Alignment tool [12]. Likely PCR duplicates were removed with the Picard program (http://picard.sourceforge.net/). Single-nucleotide variants and indels were identified using the Genome Analysis Tool Kit (GATK) v1.6 software [13]. SNVs and indels were annotated against the RefSeq database, 1000 Genomes Project variant data, and dbSNP135 with the ANNOVAR program [14].

To confirm mutations indicated by exome sequencing, Sanger sequencing was performed for PCR products obtained with primers flanking the detected mutations, using a 3500xL genetic analyzer (Life Technologies). Furthermore, the PCR products were subcloned with TOPO TA Cloning Kit (Life Technologies), and normal and mutant alleles were sequenced separately.

In silico protein functional analysis

Function of proteins with missense variations was assessed by Polymorphism Phenotyping-2 (PolyPhen-2, http://genetics.bwh.harvard.edu/pph2/) and Sorting Intolerant From Tolerant (SIFT, http://sift.jcvi.org/), and that of proteins with in-frame amino acid deletions was evaluated by PROVEAN predictions (http://provean.jcvi.org/index.php).

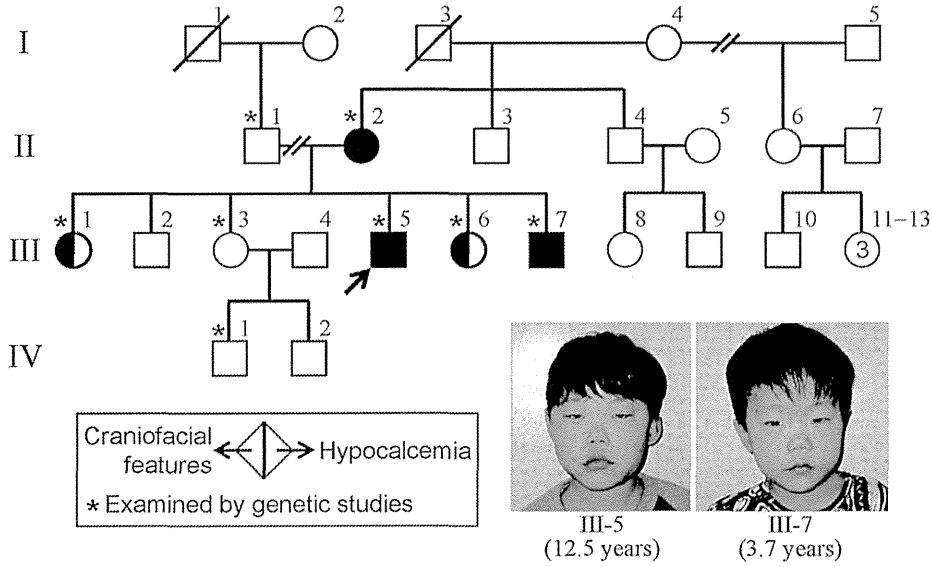

Figure 1. The pedigree of this family. Facial features of subjects III-5 and III-7 are shown.
doi:10.1371/journal.pone.0091598.g001

Results

FISH and Array CGH Analyses

FISH analysis delineated two signals for *HIRA* (Fig. 2A). Array CGH analysis revealed no copy number change specific to group 1 or groups 1+2, in the entire genome including chromosome 10p13-14 and chromosome 22q11.2 regions (Fig. 2B).

Exome and Sanger Sequencings

Exome sequencing identified nine heterozygous non-synonymous variants (six missense variants, two in-frame microdeletions, and one frameshift variant) that were specific to groups 1+2 (namely, they were present in groups 1+2 and absent from group 3 as well as from 1000 Genomes, dbSNP135, and our in-house exome data from 70 individuals) (Table S1). Notably, the frameshift variant (c.1253delA, p.Y418fsX459) was found at exon 9C of *TBX1* for DGS/VCFS (Fig. 3). Of the remaining eight variants, two variants were also detected in disease-related genes: p.G204R in *HDAC4* for brachydactyly-mental retardation syndrome [15], and p.276del in *CCND1* constituting a susceptibility factor for colorectal cancer and a modifier for von Hippel-Lindau disease [16,17]. Exome sequencing also detected two heterozygous missense variants that were specific to group 1 (Table S1).

When all variants were included, exome sequencing revealed: (1) 83 non-synonymous and 86 synonymous variants that were present in groups 1+2 and absent from group 3 (Table S2); (2) 54 non-synonymous and 48 synonymous variants that were present in group 1 and absent from groups 2+3 (Table S3); (3) 6,033 non-synonymous and 6,667 synonymous variants that were present in groups 1+2, but not specific to groups 1+2 (thus, they may be present in group 3 or absent from group 3); and (4) 7,073 non-synonymous and 7,861 synonymous variants that were present in group 1, but not specific to group 1. Furthermore, comparison of the exome sequencing data between group 1 with hypocalcemia and group 2 without hypocalcemia revealed 231 non-synonymous and 254 synonymous variants that were present in group 1 and absent from group 2 (Table S4), and 246 non-synonymous and 242 synonymous variants that were present in group 2 and absent from group 1 (Table S5). (The variant data other than those described in Supplemental Tables may be available on request after discussion with the family members and approval by our IRBs, because they contain a huge amount of individual genetic information.)

In silico protein functional analysis

The results are summarized in Table S1. The p.G204R in *HDAC4* and the p.E276del in *CCND1* were assessed as non-pathologic, while some variants were evaluated as potentially pathologic.

Discussion

Exome sequencing successfully identified a heterozygous frameshift variant on exon 9C of *TBX1*. The c.1253delA (p.Y418fsX459) appears to be a disease-causing mutation, because it is predicted that this variant escapes nonsense-mediated mRNA decay due to its position on the final exon [18] and produces a truncated protein lacking the nuclear localization signal (NLS) and most of the transactivation domain (TAD) on exon 9C (Fig. 3) [19]. In support of this, functional studies for a similar c.1223delC (p.S408fsX459) mutation on exon 9C have shown that the truncated p.S408fsX459 protein was incapable of localizing to nucleus and lost transactivation function [2,5,19]. One may argue that this c.1253delA mutation affects *TBX1* isoform C (*TBX1C*, TBX1-003) alone, while *TBX1* produces three transcript variants containing T-box [2,4] (Fig. 3). However, *TBX1C* is the major transcript with the NLS and the TAD in human and is highly homologous to mouse *Tbx1* [4] (Fig. S1).

Craniofacial features in groups 1+2 and hypocalcemia in group 1 are well explained by the *TBX1* mutation [3]. This argues for a critical role of this mutation in the phenotypic development in groups 1+2, while the clinical effects of the remaining variants identified by exome sequencing are largely unknown. In this regard, comparison between group 1 with hypocalcemia and group 2 without hypocalcemia revealed a large number of non-synonymous and synonymous variants that exclusively belonged to either group 1 (Table S4) or group 2 (Table S5), although the lists did not contain a c.2968A>G (p.R990G) SNP in *CASR* (calcium sensing receptor) that has a gain-of-function effect and appears to raise the susceptibility to hypocalcemia (Fig. S2) [20]. Thus, it is

Table 1. Clinical findings of the family members.

	TBX1 mutation (+)					*TBX1* mutation (−)			*TBX1* mutation (N.E.)		
Individual	**II-2**	**III-1**	**III-5**	**III-6**	**III-7**	**II-1**	**III-3**	**IV-1**	**II-3**	**II-4**	**III-2**
Present age (year)	51	26	19	13	10	59	22	5	50	49	25
Sex	F	F	M	F	M	M	F	M	M	M	M
Craniofacial features	+	+	+	+	+	−	−	−	−	−	−
Hypertelorism	+	+	+	+	+	−	−	−	−	−	−
Blepharophimosis	+	+	+	+	+	−	−	−	−	−	−
Low set ears	+	+	+	+	+	−	−	−	−	−	−
Auricular anomalies	+	−	−	−	−	−	−	−	−	−	−
Narrow nose	+	+	+	+	+	−	−	−	−	−	−
Cleft palate	−	−	−	−	−	−	−	−	−	−	−
Micrognathia	±	+	+	+	+	−	−	−	−	−	−
Velopharyngeal incompetence	+[d]	+	+	+	+	−	−	−	−	−	−
Hypoparathyroidism	+	−	+	−	+	−	−	−	−	−	−
Age at examination (year)	44	17	8	4	0 (1 day)	N.E.	15	0 (6 days)	N.E.	N.E.	18
Serum calcium (mg/dL)[a]	7.6[e]	9.0	6.0	9.1	5.9	...	9.0	9.8	...	...	9.6
Serum i-phosphate (mg/dL)[a]	3.9[e]	4.9	9.1	5.0	N.E.	...	4.8	6.3	...	...	4.6
Serum intact PTH (pg/dL)[a]	31[e]	N.E.	15	N.E.	19	...	N.E.	34	...	...	N.E.
Cardiovascular anomalies[b]	−	−	−	−	−	−	−	−	−	−	−
Hypoplastic thymus[c]	−	N.E.	N.E.	N.E.	N.E.	N.E.	N.E.	N.E.	N.E.	N.E.	N.E.
Susceptible to infection	−	−	−[f]	−	−	−	−	−	−	−	−
Other features	−	−	−	−	−	−	−	−	−	−	−
Developmental retardation	+	+	+[g]	+	+[g]	−	−	−	−	−	−
Sensorineural deafness	+[h]	−	−	−	−	−	−	−	−	−	−
Graves' disease	−	−	+[i]	−	−	−	−	−	−	−	−

Individuals correspond to those shown in Fig. 1.
i-phosphate: inorganic phosphate; SD: standard deviation; F: female; M: male; and N.E.: not examined.
[a]Reference values: calcium, 9.0–11.0 mg/dL in infants and 8.8–10.2 mg/dL in adults; inorganic phosphate, 4.8–7.5 mg/dL in infants and 2.5–4.5 mg/dL in adults, and intact PTH, 10–65 pg/dL in infants and 14–55 pg/dL in adults.
Conversion factor to the SI unit: 0.25 for calcium (mmol/L), 0.32 for inorganic phosphate (mmol/L), and 0.106 for intact PTH (pmol/L).
[b]Examined by echocardiography, chest roentgenography, and/or electrocardiography.
[c]Examined by computed tomography.
[d]Received velopharyngeal closure.
[e]On treatment with vitamin D.
[f]Repeated otitis media only.
[g]Received speech therapy.
[h]Required hearing aids.
[i]At the time of diagnosis (11 years of age), serum TSH was <0.01 mIU/L, free T_3 33.1 pg/mL [51.0 pmol/L], free T_4 5.11 ng/dL [65.8 nmol/L], and TSH receptor antibody 1284% [normal range <1.9%].
doi:10.1371/journal.pone.0091598.t001

likely that, together with environmental factors, the combination of hitherto unknown calcium metabolism-related functional variants would underlie different serum calcium values between groups 1 and 2.

In addition to craniofacial features with and without hypocalcemia, *TBX1* mutation positive subject II-2 had sensorineural deafness, and III-5 had Graves' disease. Since such features are occasionally manifested by patients with 22q11.2DS [21,22], the results may suggest the relevance of *TBX1* to such rather infrequent features in 22q11.2DS.

The five *TBX1* mutation positive subjects in groups 1+2 lacked cardiovascular lesion and manifested borderline to mild developmental retardation (while they had no susceptibility to infection, assessment of thymic hypoplasia remained fragmentary). By contrast, cardiovascular lesion is frequently observed and developmental retardation is rare in previously reported patients with *TBX1* mutations, although clinical features are fairly variable among mutation positive patients (Table 2). Such difference would more or less be ascribed to an examination bias that *TBX1* has been analyzed in patients with isolated cardiovascular lesion in several studies [4,6,7] or to the functional difference of the mutant proteins [2,5–8]. However, in seven patients who have been examined for DGS/VCFS-like clinical features and found to have frameshift mutations on exon 9C (p.S408fsX459, p.H425fsX613, and p.S431fsX608) affecting the NLS and the TAD, cardiovascular lesion was present in four patients and developmental delay was absent or not described, despite apparent similarity in the ascertainment of patients and the function of mutant proteins between the seven patients and the five affected subjects in this family (Table 2) [2–5].

Thus, there may be protective factor(s) for cardiovascular lesion and susceptibility factor(s) for developmental delay in groups 1+2.

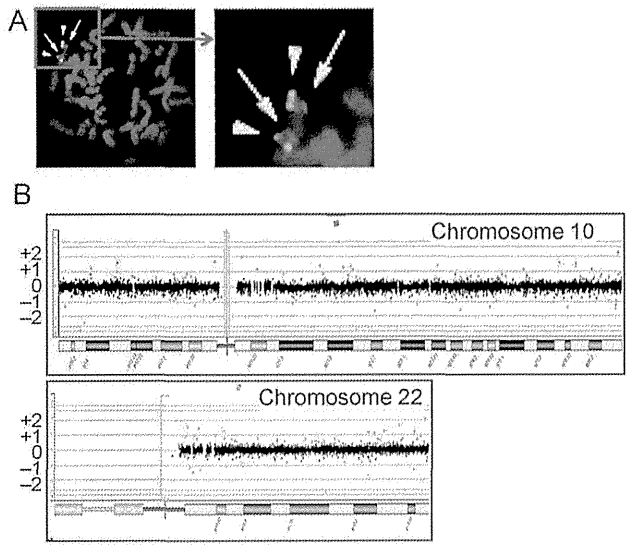

Figure 2. FISH and array CGH analyses in the proband (III-5). A. FISH analysis. Two signals are shown for both *HIRA* at 22q11.2 (red signals indicated by arrows) and *ARSA* at 22q13 (green signals indicated by arrowheads). **B.** Array CGH analysis. No copy number change is found for chromosome 10 carrying the second DiGeorge region and chromosome 22 harboring the DGS/VCFS critical region, as well as other chromosomes (not shown). Black, red, and green dots denote signals indicative of the normal, the increased (>+0.5), and the decreased (<−0.8) copy numbers, respectively. Although several red and green signals are seen, there is no portion associated with ≥3 consecutive red or green signals.
doi:10.1371/journal.pone.0091598.g002

In this regard, a simple explanation would be that protective factor(s) for cardiovascular lesion are present in groups 1+2 and may be present in group 3 or absent from group 3, whereas susceptibility factor(s) for developmental delay is present in groups 1+2 and absent from group 3. Since 6,033 non-synonymous and 6,667 synonymous variants were found to be present in groups 1+2 but not specific to groups 1+2, and 83 non-synonymous and 86 synonymous variants were revealed to be present in groups 1+2 and absent from group 3, a certain fraction of functional variants may constitute protective factor(s) for cardiovascular lesion and susceptibility factor(s) for developmental delay. In addition, while p.G204R on *HDAC4* for brachydactyly-mental retardation syndrome was assessed as non-pathologic by *in silico* analysis, it may have played a certain role in the occurrence of developmental delay in groups 1+2. Actually, such protective and susceptibility factor(s) would be more complex, with the effects of functional variants unique to each patient as well as the influences of environmental factors. Furthermore, it remains possible that the c.1253delA (p.Y418fsX459) mutation found in this study may be related to a specific phenotype characterized by the presence of craniofacial features and developmental delay and by the absence of cardiovascular lesion, because of a hitherto unrevealed mechanism(s). This matter awaits further studies.

Besides the clinical findings, several matters are also notable in the nine apparently pathologic *TBX1* mutations identified to date (Table 2). First, the mutations reside on exons 3–8 common to isoforms A–C or on exon 9C specific to isoform C, with no mutation on exons 9A and 9B specific to isoforms A and B. This would be consistent with *TBX1C* having the primary biological function. Second, while most mutations have loss-of-function effects, gain-of-function effects have been suggested for p.F148Y, p.H194Q, and p.310S by *in vitro* studies [8]. Thus, *TBX1* loss-of-function mutations and gain-of-function mutations may result in overlapping clinical features. Lastly, the c.1274_1281delACTATCTC (p.H425fsX613) missing the NLS on exon 9C was shared by a patient with DGS-like phenotype and the apparently normal mother, and the c.129_185del57 (p.43-61del19) with reduced transcriptional activity was common to a patient with non-syndromic tetralogy of Fallot and the apparently normal mother. This would imply the reduced penetrance of phenotypes caused by these mutations.

In summary, we identified a *TBX1* mutation by exome sequencing in a family with chromosome 22q11.2 deletion-like

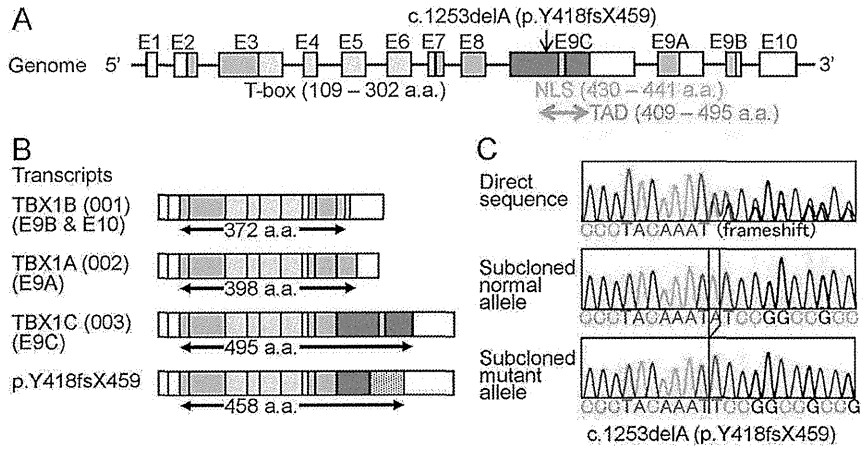

Figure 3. *TBX1* mutation identified in this family. A. Genomic structure of *TBX1* and the position of the mutation. The color and the white boxes represent the coding regions and the untranslated regions on exons 1–10 (E1–E10), respectively; the red, the purple, and the orange segments indicate the coding regions on the final exons 9C, 9A, and 9B (splice variants), respectively. The T-box is indicated by yellow boxes, the nuclear localization signal (NLA) by a blue segment, and the transactivation domain (TAD) by a green arrow. The c.1253delA (p.Y418fsX459) identified in this family resides on exon 9C. **B.** Transcripts of *TBX1*. Three variants are formed by alternative splicing of the final exons 9C, 9A, and 9B. The c.1253delA (p.Y418fsX459) mutation is predicted to yield a truncated TBX1C protein missing the NLS and most of the TAD. The stippled box of p.Y418fsX459 denotes aberrant amino acid sequence produced by the frameshift mutation. **C.** Electrochromatograms showing the frameshift mutation by Sanger sequencing. The primer sequences used are: 5′-GCGGCCAAGAGCCTTCTCT-3′ and 5′-GGGTGGTAGCCGTGGCCA-3′.
doi:10.1371/journal.pone.0091598.g003

Table 2. Summary of patients with *TBX1* mutations.

	TBX1C only					TBX1A–C				22q11.2DS
Position	**Exon 9C**	**Exon 9C**	**Exon 9C**	**Exon 9C**	**Exon 9C**	**Exon 3**	**Exon 4**	**Exon 5**	**Exon 8**	
cDNA change[a]	c.1223	c.1253	c.1274_1281	c.1293_1315	c.1399_1428	c.129_185	c.443T>A	c.582C>G	c.928G>A	Deletion
	delC	delA	del8	del23[h]	dup30[k]	del57[k]				
Amino acid	p.S408	p.Y418	p.H425	p.S431	p.467_476	p.43_61	p.F148Y	p.H194Q	p.G310S	
change	fsX459	fsX459	fsX613	fsX608	dup10A	del19				
NLS (exon 9C)	–	–	–	+[i]	+[l]	+	+	+	+	
TAD (exon 9C)	–	Involved	Involved	Involved	Involved	+	+	+	+	
Function	LOF	N.E.	N.E.	LOF	LOF	Reduced	GOF[m]	GOF[m]	GOF[m]	
Patient number	3	5	1	3[j]	2	1	1	2	1	558
Occurrence	Familial	Familial	Sporadic[g]	Familial	Sporadic	Sporadic[g]	Sporadic	Familial	Sporadic	
Facial features[b]	3/3	5/5	+	3/3	0/2	–	+	2/2	+	100%
Nasal voice[c]	2/3	5/5	N.D.	3/3	0/2	–	+	0/2	+	32%
Cardiovascular anomalies	1/3	0/5	+	2/3	2/2	+	+	0/2	+	57%
Hypopara-thyroidism[d]	1/3	3/5	+	N.D.	0/2	–	–	0/2	+	60%
Hypoplastic thymus	1/2[e]	0/1[f]	+	N.D.	0/2	–	–	N.E.	+	?
Susceptible to infection	N.D.	0/5	N.D.	N.D.	0/2	–	N.D.	N.D.	N.D.	?
Developmental retardation	0/3	5/5	N.D	0/3	0/2	–	–	1/2	–	38%
Reference	2	This study	3, 4	5	4, 6	7	2	8	2	1

In addition to the mutations listed in this table, several missense variants and in-frame indels with unknown functions have been found in patients with isolated cardiovascular anomalies and in those with DGS/VCFS-like phenotype [4].
NLS: nuclear localization signal; TAD: transactivation domain; LOF: loss-of-function; N.D.: not described; N.E.: not examined; GOF: gain-of-function; Del: deletion; and Dup: duplication.
[a]According to NM_080647.
[b]Suggestive of 22q11.2 deletion syndrome.
[c]Velopharygeal insufficiency.
[d]Hypocalcemia is included.
[e]Two of the three subjects have been examined for hypoplastic thymus.
[f]One of the five subjects has been examined for hypoplastic thymus.
[g]These two mutations have been inherited from apparently normal mothers.
[h]The c.1293-1315del23 has been described as c.1320-1342del23 in the original report [5].
[i]Although the natural NLS has been disrupted, a new NLS-compatible motif (RGRRRRCR) has been created on the added amino acid sequence.
[j]Another deceased individual in this family also has similar clinical features.
[k]These two mutations have been identified in *TBX1* analyses for patients with cardiovascular anomalies only.
[l]The mutant protein is aggregated in the cytoplasm and the nucleus.
[m]Gain-of-function effects have been found by *in vitro* studies [8].
doi:10.1371/journal.pone.0091598.t002

phenotype. Application of such powerful methods will serve to identify a causative gene in genetically heterogeneous disorders.

Supporting Information

Figure S1 Comparison of amino acid sequence of human *TBX1C* and mouse *Tbx1*. The T-box is highlighted in yellow, and the nuclear localization signal in light blue. The region for transactivation domain is surrounded by squares. The Y highlighted in red denotes the amino acid residue where the frameshift mutation in this family has taken place.
(TIF)

Figure S2 Analysis of c.2968A>G SNP (p.R990G, rs1042636) with a gain-of-function effect in exon 7 of *CASR*. The SNP pattern is not co-segregated with the presence or absence of hypocalcemia.
(TIF)

Table S1 Summary of heterozygous non-synonymous variants.
(PDF)

Table S2 A list of variants that are present in groups 1+2 and absent from group 3.
(PDF)

Table S3 A list of variants that are present in group 1 and absent from groups 2+3.
(PDF)

Table S4 A list of variants that are present in group 1 and absent from group 2.
(PDF)

Table S5 A list of variants that are present in group 2 and absent from group 1.
(PDF)

References

1. Ryan AK, Goodship JA, Wilson DI, Philip N, Levy A, et al. (1997) Spectrum of clinical features associated with interstitial chromosome 22q11 deletions: a European collaborative study. J Med Genet 34: 798–804.
2. Yagi H, Furutani Y, Hamada H, Sasaki T, Asakawa S, et al. (2003) Role of TBX1 in human del22q11.2 syndrome. Lancet 362: 1366–1373.
3. Baldini A (2005) Dissecting contiguous gene defects: TBX1. Curr Opin Genet Dev 15: 279–84.
4. Gong W, Gottlieb S, Collins J, Blescia A, Dietz H, et al. (2001) Mutation analysis of TBX1 in non-deleted patients with features of DGS/VCFS or isolated cardiovascular defects. J Med Genet 38: E45.
5. Paylor R, Glaser B, Mupo A, Ataliotis P, Spencer C, et al. (2006) Tbx1 haploinsufficiency is linked to behavioral disorders in mice and humans: implications for 22q11 deletion syndrome. Proc Natl Acad Sci U S A 103: 7729–7734.
6. Rauch R, Hofbeck M, Zweier C, Koch A, Zink S, et al. (2010) Comprehensive genotype-phenotype analysis in 230 patients with tetralogy of Fallot. J Med Genet 47: 321–331.
7. Griffin HR, Töpf A, Glen E, Zweier C, Stuart AG, et al. (2010) Systematic survey of variants in TBX1 in non-syndromic tetralogy of Fallot identifies a novel 57 base pair deletion that reduces transcriptional activity but finds no evidence for association with common variants. Heart 96: 1651–1655.
8. Zweier C, Sticht H, Aydin-Yaylagül I, Campbell CE, Rauch A (2007) Human TBX1 missense mutations cause gain of function resulting in the same phenotype as 22q11.2 deletions. Am J Hum Genet 80: 510–517.
9. Daw SCM, Taylor C, Kraman M, Call K, Mao J, et al. (1996) A common region of 10p deleted in DiGeorge and velocardiofacial syndromes. Nat Genet 13: 458–461.
10. McDonnell SK, Riska SM, Klee EW, Thorland EC, Kay NE, et al. (2013) Experimental designs for array comparative genomic hybridization technology. Cytogenet Genome Res 139: 250–257.
11. Wang Z, Liu X, Yang B-Z, Gelernter J (2013) The role and challenges of exome sequencing in studies of human diseases Front Genet doi: 10.3389/fgene.2013.00160.
12. Li H, Durbin R (2009) Fast and accurate short read alignment with Burrows-Wheeler transform. Bioinformatics 25: 1754–1760.
13. McKenna A, Hanna M, Banks E, Sivachenko A, Cibulskis K, et al. (2010) The Genome Analysis Toolkit: a MapReduce framework for analyzing next-generation DNA sequencing data. Genome Res 20: 1297–1303.
14. Wang K, Li M, Hakonarson H (2010) ANNOVAR: functional annotation of genetic variants from high-throughput sequencing data. Nucleic Acids Res 38: e164.
15. Williams SR, Aldred MA, Der Kaloustian VM, Halal F, Gowans G, et al (2010). Haploinsufficiency of HDAC4 causes brachydactyly mental retardation syndrome, with brachydactyly type E, developmental delays, and behavioral problems. Am J Hum Genet 87: 219–228.
16. Kong S, Amos CI, Luthra R, Lynch PM, Levin B, et al. (2000) Effects of cyclin D1 polymorphism on age of onset of hereditary nonpolyposis colorectal cancer. Cancer Res 60: 249–252.
17. Zatyka M, da Silva NF, Clifford SC, Morris MR, Wiesener MS, et al (2002). Identification of cyclin D1 and other novel targets for the von Hippel-Lindau tumor suppressor gene by expression array analysis and investigation of cyclin D1 genotype as a modifier in von Hippel-Lindau disease. Cancer Res 62: 3803–3811.
18. Holbrook JA, Neu-Yilik G, Hentze MW, Kulozik AE (2004) Nonsense-mediated decay approaches the clinic. Nat Genet 36: 801–808.
19. Stoller JZ, Epstein JA (2005) Identification of a novel nuclear localization signal in Tbx1 that is deleted in DiGeorge syndrome patients harboring the 1223delC mutation. Hum Mol Genet 14: 885–892.
20. Vezzoli G, Terranegra A, Arcidiacono T, Biasion R, Coviello D, et al. (2007) R990G polymorphism of calcium-sensing receptor does produce a gain-of-function and predispose to primary hypercalciuria. Kidney Int 71: 1155–1162.
21. Ohtani I, Schuknecht HF (1984) Temporal bone pathology in DiGeorge's syndrome. Ann Otol Rhinol Laryngol 93(3 Pt 1): 220–224.
22. Kawame H, Adachi M, Tachibana K, Kurosawa K, Ito F, et al. (2001) Graves' disease in patients with 22q11.2 deletion. J Pediatr 139: 892–895.

Author Contributions

Conceived and designed the experiments: TO YM. Performed the experiments: T. Niihori SN FK MF YA. Analyzed the data: T. Nagashima RF KN. Contributed reagents/materials/analysis tools: KN. Wrote the manuscript: TO. Collected the clinical findings: NT MK.

International Journal of Cardiology 173 (2014) e63–e66

Contents lists available at ScienceDirect

International Journal of Cardiology

journal homepage: www.elsevier.com/locate/ijcard

Letter to the Editor

Bilateral giant coronary aneurysms in a 40-year-old male with Noonan syndrome caused by a *KRAS* germline mutation

Naoki Fujimoto [a,*], Hiroshi Nakajima [b], Emiyo Sugiura [b], Kaoru Dohi [b], Shinji Kanemitsu [c], Norikazu Yamada [b], Yoko Aoki [d], Kaname Nakatani [a], Hideto Shimpo [c], Tsutomu Nobori [a], Masaaki Ito [b]

[a] Department of Molecular and Laboratory Medicine, Mie University Graduate School of Medicine, Tsu, Japan
[b] Department of Cardiology and Nephrology, Mie University Graduate School of Medicine, Tsu, Japan
[c] Department of Thoracic and Cardiovascular Surgery, Mie University Graduate School of Medicine, Tsu, Japan
[d] Department of Medical Genetics, Tohoku University School of Medicine, Sendai, Japan

ARTICLE INFO

Article history:
Received 7 February 2014
Accepted 15 March 2014
Available online 21 March 2014

Keywords:
Noonan syndrome
Coronary aneurysm
KRAS germline mutation

We report a case of a 40-year-old man who was admitted to our hospital for the evaluation and treatment of chest discomfort on exertion. He had previously been followed for post-natal growth deficiency, strabismus, mental retardation, epilepsy, and moderate mitral regurgitation. On admission, he was 142 cm in height and 42 kg in weight. Physical examination revealed orbital hypertelorism, ptosis, a webbed neck, and low-set ears with no jugular vein dilatation or peripheral edema. Cardiac auscultation showed a 3/6 late systolic murmur and S4. ECG showed normal sinus rhythm, poor R wave progression in the precordial leads, and an incomplete right bundle brunch block. Chest X-ray showed pulmonary congestion and marked cardiomegaly, with a cardio-thoracic ratio of 71%.

Echocardiography revealed severe mitral regurgitation due to prolapse of the anterior and posterior mitral leaflets (Fig. 1A–C) and aneurysms near the left coronary artery (LCA) (Fig. 1D), and the right coronary artery (RCA). No left ventricular hypertrophy, wall motion abnormality, or atrial septal defects were observed. A CT scan also revealed coronary aneurysms with no pulmonic stenosis; one aneurysm near the LCA measured 40 × 32 mm, and the other near the RCA 13 × 12 mm (Fig. 2A–B). Total occlusion of right common iliac artery with subsequent aneurysmal change, and dilatation of left common iliac artery were observed. Coronary angiography was then performed to elucidate the complex anatomy of the aneurysms and coronary arteries (Fig. 2C–D). A giant aneurysm containing a thrombus originated from the proximal LCA (Fig. 3 A–B). The left anterior descending artery was occluded with small collaterals from the left circumferential artery (LCX). The other aneurysm originated from the proximal RCA (Fig. 3 C–D), and the distal portion of the RCA was occluded with collaterals from the LCX.

It was thought that severe mitral regurgitation from a prolapsed leaflet and myocardial ischemia due to coronary aneurysms and severe occlusive coronary artery disease were responsible for his symptoms. The patient underwent a surgical procedure that involved mitral valve repair, ligation of the aneurysms, and coronary artery bypass grafting. The post-operative course was complicated by ventricular fibrillation during the operation and the patient unfortunately expired due to refractory congestive heart failure 13 days after surgery.

Genetic screening confirmed a heterozygous nucleotide change within exon 4b of the *KRAS* gene (c.458A>T), causing the amino acid substitution D153V, whose clinical phenotype was Noonan/Cardio-facio-cutaneous (CFC) syndrome [1,2].

Noonan syndrome was first described in 1963, and CFC syndrome was described in 1986. These syndromes have many overlapping manifestations such as short stature, characteristic facial appearance, mental retardation and heart abnormalities, including pulmonic stenosis, hypertrophic cardiomyopathy, and atrial septal defects. While, coronary aneurysms with occlusive coronary artery disease, as seen in our case, have been rarely reported in an adult patient with these syndromes [3]. Moreover, it was unclear when and how these cardiovascular changes had occurred during his life. We conclude that patients with Noonan/CFC syndrome may have the risks for coronary aneurysms and severe cardiovascular disease. Thus, careful cardiovascular follow-up should be performed in their entire life.

References

[1] Schubbert S, Zenker M, Rowe SL, et al. Germline KRAS mutations cause Noonan syndrome. Nat Genet 2006;38:331–6.
[2] Niihori T, Aoki Y, Narumi Y, et al. Germline KRAS and BRAF mutations in cardio-facio-cutaneous syndrome. Nat Genet 2006;38:294–6.
[3] Loukas M, Dabrowski M, Kantoch M, Ruzyłło W, Waltenberger J, Giannikopoulos P. A case report of Noonan's syndrome with pulmonary valvar stenosis and coronary aneurysms. Med Sci Monit 2004;10:CS80–3.

* Corresponding author at: Department of Molecular and Laboratory Medicine, Mie University Graduate School of Medicine, 2-174 Edobashi, Tsu 514-8507, Japan. Tel.: +81 59 231 5161; fax: +81 59 231 5250.
E-mail address: naokifujimo@clin.medic.mie-u.ac.jp (N. Fujimoto).

http://dx.doi.org/10.1016/j.ijcard.2014.03.135

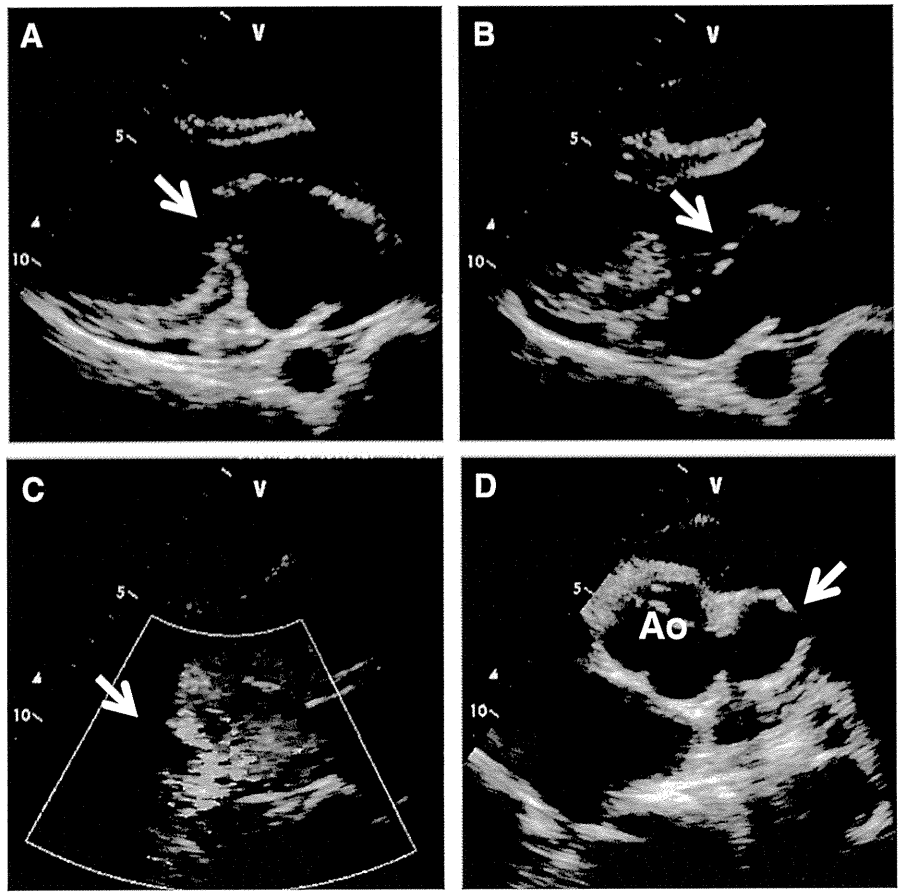

Fig. 1. Two-dimensional echocardiogram at end-diastole (A) and end-systole (B–C) showing severe mitral regurgitation due to mitral prolapse (arrow). Short axis image at the level of aortic valve with a giant aneurysm near left coronary artery (D).

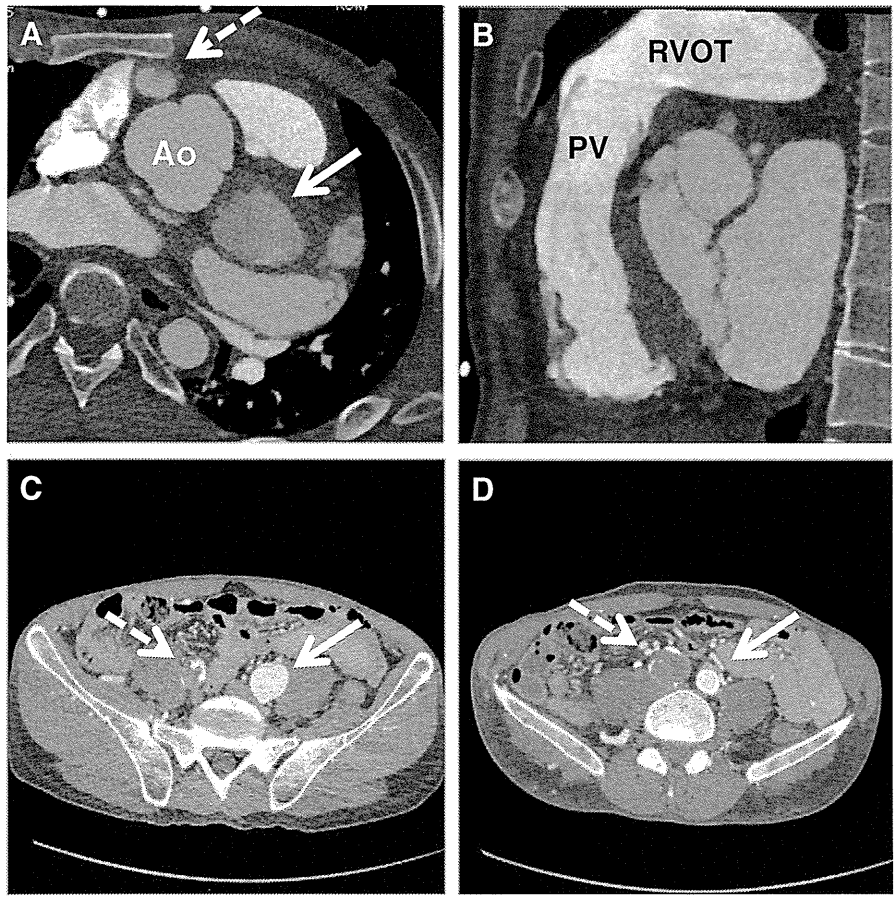

Fig. 2. Computed tomography (CT) axial view showing aneurysms near left coronary artery (arrow) and the right coronary artery (broken arrow)(A). CT sagittal view with intact pulmonic valve (PV) and right ventricular outflow tract (RVOT). CT axial view at proximal (C) and distal (D) levels of common iliac artery showing occluded right common iliac artery (broken arrow) and dilated left common iliac artery (arrow).

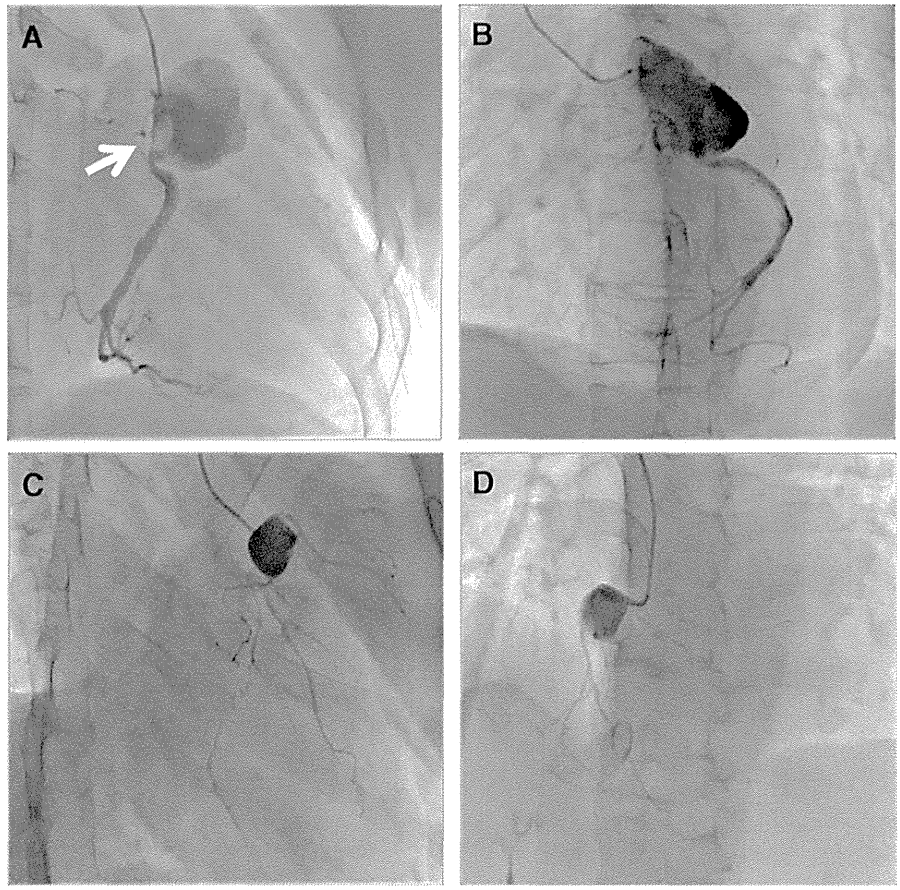

Fig. 3. Left coronary artery angiography in right anterior oblique (RAO; panel A) and left anterior oblique (LAO) views (panel B) showing a giant left coronary aneurysm containing a thrombus near the origin of the left circumflex coronary artery (arrow). Right coronary artery angiography in RAO caudal (C) and LAO cranial (D) views showing a right coronary aneurysm and coronary artery stenosis.

Human Molecular Genetics, 2014, Vol. 23, No. 16 **4315–4327**
doi:10.1093/hmg/ddu148
Advance Access published on April 4, 2014

Activating mutations in *RRAS* underlie a phenotype within the RASopathy spectrum and contribute to leukaemogenesis

Elisabetta Flex[1,†], Mamta Jaiswal[3,†], Francesca Pantaleoni[1,‡], Simone Martinelli[1,‡], Marion Strullu[4,7,‡], Eyad K. Fansa[3,‡], Aurélie Caye[4,7], Alessandro De Luca[8], Francesca Lepri[9], Radovan Dvorsky[3], Luca Pannone[1], Stefano Paolacci[1], Si-Cai Zhang[3], Valentina Fodale[1], Gianfranco Bocchinfuso[10], Cesare Rossi[11], Emma M.M. Burkitt-Wright[12], Andrea Farrotti[10], Emilia Stellacci[1], Serena Cecchetti[2], Rosangela Ferese[8], Lisabianca Bottero[1], Silvana Castro[13], Odile Fenneteau[5], Benoît Brethon[6], Massimo Sanchez[2], Amy E. Roberts[14], Helger G. Yntema[15], Ineke Van Der Burgt[15], Paola Cianci[16], Marie-Louise Bondeson[17], Maria Cristina Digilio[9], Giuseppe Zampino[18], Bronwyn Kerr[12], Yoko Aoki[19], Mignon L. Loh[20], Antonio Palleschi[10], Elia Di Schiavi[13,¶], Alessandra Carè[1], Angelo Selicorni[16], Bruno Dallapiccola[9], Ion C. Cirstea[3,21], Lorenzo Stella[10], Martin Zenker[22], Bruce D. Gelb[23,24,25], Hélène Cavé[4,7,§], Mohammad R. Ahmadian[3,§] and Marco Tartaglia[1,§,*]

[1]Dipartimento di Ematologia, Oncologia e Medicina Molecolare and [2]Dipartimento di Biologia Cellulare e Neuroscienze, Istituto Superiore di Sanità, Rome 00161, Italy, [3]Institut für Biochemie und Molekularbiologie II, Medizinische Fakultät der Heinrich-Heine Universitat, Düsseldorf 40225, Germany, [4]Genetics Department, [5]Biological Hematology Department and [6]Pediatric Hematology Department, Robert Debré Hospital, Paris 75019, France, [7]INSERM UMR_S940, Institut Universitaire D'Hématologie (IUH), Université Paris-Diderot Sorbonne-Paris-Cité, Paris 75010, France, [8]Laboratorio Mendel, Istituto di Ricovero e Cura a Carattere Scientifico-Casa Sollievo Della Sofferenza, Rome 00198, Italy, [9]Ospedale Pediatrico 'Bambino Gesù', Rome 00165, Italy, [10]Dipartimento di Scienze e Tecnologie Chimiche, Università 'Tor Vergata', Rome 00133, Italy, [11]UO Genetica Medica, Policlinico S.Orsola-Malpighi, Bologna 40138, Italy, [12]Genetic Medicine, Academic Health Science Centre, Central Manchester University Hospitals NHS Foundation Trust, Manchester M13 9WL, UK, [13]Istituto di Genetica e Biofisica 'A. Buzzati Traverso', Consiglio Nazionale Delle Ricerche, Naples 80131, Italy, [14]Department of Cardiology and Division of Genetics, and Department of Medicine, Boston Children's Hospital, Boston, MA 02115, USA, [15]Department of Human Genetics, Radboud University Medical Centre, and Nijmegen Centre for Molecular Life Sciences, Radboud University, Nijmegen 6500, The Netherlands, [16]Genetica Clinica Pediatrica, Clinica Pediatrica Università Milano Bicocca, Fondazione MBBM, A.O. S. Gerardo, Monza 20900, Italy, [17]Department of Immunology, Genetics and Pathology, Uppsala University, Uppsala 75237, Sweden, [18]Istituto di Clinica Pediatrica, Università Cattolica del Sacro Cuore, Rome 00168, Italy, [19]Department of Medical Genetics, Tohoku University School of Medicine, Sendai 980-8574, Japan, [20]Department of Pediatrics, Benioff Children's Hospital, University of California School of Medicine, and the Helen Diller Family Comprehensive Cancer Center, San Francisco, CA 94143, USA, [21]Leibniz Institute for Age Research, Jena 07745, Germany, [22]Institute of Human Genetics, University Hospital of

*To whom correspondence should be addressed at: Dipartimento di Ematologia, Oncologia e Medicina Molecolare, Istituto Superiore di Sanità, Viale Regina Elena, 299, 00161 Rome, Italy. Tel: +39 0649902569; Fax: +39 0649902850; Email: marco.tartaglia@iss.it
†These authors contributed equally to this project.
‡These authors contributed equally to this project.
¶Present address: Institute of Bioscience and BioResources, Consiglio Nazionale delle Ricerche, Naples 80131, Italy.
§These authors contributed equally as the senior investigators for this project.

Magdeburg, Otto-von-Guericke-University, Magdeburg 39120, Germany, [23]Department of Pediatrics and [24]Department of Genetics and [25]Department of Genomic Sciences, Mindich Child Health and Development Institute, Icahn School of Medicine at Mount Sinai, New York, NY 10029, USA

Received December 10, 2013; Revised and Accepted March 4, 2014

RASopathies, a family of disorders characterized by cardiac defects, defective growth, facial dysmorphism, variable cognitive deficits and predisposition to certain malignancies, are caused by constitutional dysregulation of RAS signalling predominantly through the RAF/MEK/ERK (MAPK) cascade. We report on two germline mutations (p.Gly39dup and p.Val55Met) in *RRAS*, a gene encoding a small monomeric GTPase controlling cell adhesion, spreading and migration, underlying a rare (2 subjects among 504 individuals analysed) and variable phenotype with features partially overlapping Noonan syndrome, the most common RASopathy. We also identified somatic *RRAS* mutations (p.Gly39dup and p.Gln87Leu) in 2 of 110 cases of non-syndromic juvenile myelomonocytic leukaemia, a childhood myeloproliferative/myelodysplastic disease caused by upregulated RAS signalling, defining an atypical form of this haematological disorder rapidly progressing to acute myeloid leukaemia. Two of the three identified mutations affected known oncogenic hotspots of *RAS* genes and conferred variably enhanced RRAS function and stimulus-dependent MAPK activation. Expression of an RRAS mutant homolog in *Caenorhabditis elegans* enhanced RAS signalling and engendered protruding vulva, a phenotype previously linked to the RASopathy-causing SHOC2^{S2G} mutant. Overall, these findings provide evidence of a functional link between RRAS and MAPK signalling and reveal an unpredicted role of enhanced RRAS function in human disease.

INTRODUCTION

Signalling elicited by activated cell surface receptors and transduced through RAS proteins to the RAF/MEK/ERK and PI3K/AKT cascades is central to cell proliferation, survival, differentiation and metabolism (1,2). Owing to this nodal role, enhanced traffic through RAS proteins and their downstream effectors has been established to have a major impact on oncogenesis (3,4). This signalling network also controls early and late developmental processes (e.g. organogenesis, morphology determination, synaptic plasticity and growth), and germline mutations in a number of genes encoding transducers and modulatory proteins participating in the RAS/MAPK signalling pathway have been causally linked to Noonan syndrome (NS) (5), one of the most common diseases affecting development and growth, and a group of clinically related syndromes, the so-called RASopathies (6–8). In this family of disorders, constitutional dysregulation of RAS signalling can be caused by enhanced activation of HRAS, KRAS and NRAS (RAS proteins hereafter), aberrant function of upstream signal transducers or effectors (PTPN11/SHP2, SOS1, SHOC2, RAF1, BRAF, MAP2K1/MEK1 and MAP2K2/MEK2) or inefficient down modulation by feedback mechanisms (CBL, NF1 and SPRED1). More recently, *RIT1*, encoding a monomeric GTPase structurally linked to RAS proteins, was identified as disease gene implicated in NS (9), extending the concept of 'RASopathy gene' to a transducer that contributes to signal propagation through RAS effector pathways but does not belong to the RAS/MAPK signalling backbone.

Clinical manifestations of RASopathies include postnatal reduced growth, a wide spectrum of cardiac defects, facial dysmorphism, ectodermal and skeletal anomalies and variable cognitive deficits (5,8,10). Consistent with the key role of most RASopathy genes in oncogenesis, these disorders are also characterized by variably increased risk for certain haematologic malignancies and other paediatric cancers (6,7,11,12). Most of these conditions are genetically heterogeneous, and the underlying disease gene has not been identified yet for a still significant fraction of cases. Based on the strict mechanistic link between the molecular events controlling development and contributing to oncogenesis, these 'missing' genes represent excellent candidate oncogenes/tumour suppressors.

Here, we report that constitutional dysregulation of RRAS function is associated with a Mendelian trait within the RASopathy spectrum and that somatically acquired mutations in the same gene occur in an aggressive form of juvenile myelomonocytic leukaemia (JMML), a rare childhood myeloproliferative/myelodysplastic neoplasm representing the archetypal somatic RASopathy (13), rapidly progressing to acute myeloid leukaemia (AML). We also demonstrate that RASopathy-causing *RRAS* mutations are activating and promote signalling perturbation by enhancing stimulus-dependent MEK, ERK and, at a lower extent, AKT phosphorylation.

RESULTS

Identification of candidate disease genes and *RRAS* mutation analysis

While the core of the machinery implicated in RAS signalling has been characterized comprehensively, signal propagation through this network is likely to include a larger number of proteins playing a modulatory or structural role (14), whose aberrant or defective function is expected to perturb development and

contribute to oncogenesis. Based on this assumption, we used a protein interaction/functional association network analysis to select a panel of genes encoding proteins functionally linked to the RAS signalling network as candidates for NS or a related RASopathy (15). Candidate gene selection was based on the use of the previously identified RASopathy genes as 'seed' proteins (i.e. proteins used to build the interaction/functional networks), and considering a panel of databases to construct functional subnetworks (Supplementary material, Table S1 and Fig. S1). Sequence scanning of the best candidates in a RASopathy cohort including 96 unrelated subjects negative for mutations in known disease genes allowed the identification of a functionally relevant *RRAS* change (c.163G>A, p.Val55Met) (Supplementary material, Fig. S2) in an adult subject with clinical features suggestive of NS but lacking sufficient characteristics to allow a definitive diagnosis (Supplementary material, Table S2). Parental DNA was not available for segregation analysis. The mutation was not identified among >400 population-matched unaffected individuals, indicating that it did not represent a common polymorphic nucleotide substitution. This change, rs368625677 (dbSNP 138), had been described in 1/13,006 alleles in the NHLBI Exome Sequencing Project (http://eversusgs.washington.edu/EVS/). Of note, similar frequencies have been reported in the same database for recurrent RASopathy-causing mutations (e.g. c.922A>G in *PTPN11*, and c.1259G>A in *CBL*). Mutation analysis was extended to additional 408 patients with NS or a clinically related phenotype tested negative for mutations in the major NS disease genes (see Materials and Methods), allowing to identify one sporadic case heterozygous for a three-nucleotide duplication (c.116_118dup, p.Gly39dup) (Supplementary material, Fig. S2). Parental DNA sequencing of the relevant exon demonstrated the *de novo* origin of the variant, and STR genotyping confirmed paternity. In this subject, the duplication was documented in DNA obtained from skin fibroblasts, excluding a somatic event restricted to haematopoietic cells. The subject had features reminiscent of NS (Fig. 1A and Supplementary material, Table S2), with onset of AML suspected to represent a blast crisis of JMML (Supplementary material, Table S3 and Fig. S3). In this patient, exome sequencing performed on leukaemic and non-leukaemic DNA failed to disclose any additional relevant germline/somatic change affecting genes known to be mutated in RASopathies and JMML, as well as genes directly linked to the RAS signalling network, further supporting the causal role of the identified *RRAS* lesion. Based on this association, the occurrence of *RRAS* mutations was also explored in a panel of genomic DNAs obtained from bone marrow aspirates/circulating leukocytes of 110 subjects with JMML. Heterozygosity for the previously identified Gly^{39} duplication and the c.260A>T (p.Gln87Leu) change was observed in two patients with JMML rapidly progressing to AML (Supplementary material, Table S3 and Fig. S3). Both lesions were absent in non-leukaemic DNA, indicating their somatic origin (Supplementary material, Fig. S2). These subjects also carried a somatic *NRAS* mutation, suggesting that the two hits might cooperate with this particularly severe form of disease. Sequencing of isolated JMML myeloid colonies in patient 14385 showed that *NRAS* and *RRAS* mutations coexisted in the same progenitors but failed to establish their sequence of appearance during leukaemogenesis, not allowing to discriminate whether the latter was involved in initiation or progression of disease.

Structural analyses

RRAS encodes a 23-kD a membrane-bound monomeric GTPase with 55–60% amino acid identity to RAS proteins (16). This highly conserved structure is flanked by a unique 26-amino acid region at the *N*-terminus (Fig. 1B). Similarly to the other RAS family proteins, RRAS binds to GTP and GDP with high affinity and specificity and functions as a molecular switch by cycling between active, GTP-bound and inactive, GDP-bound states (17). RRAS is activated by guanine nucleotide exchange factors (GEFs) in response to signals elicited by cell surface receptors. In the GTP-bound state, two functionally conserved regions, switch I and switch II (Fig. 1B), undergo a conformational change enabling RRAS to bind to and activate effector proteins. This interaction is terminated by hydrolysis of GTP to GDP, which is promoted by GTPase-activating proteins (GAPs) and results in switching towards the inactive conformation. Disease-associated *RRAS* mutations affected residues highly conserved among orthologs and paralogs (Supplementary material, Fig. S4) residing in the GTP-binding pocket (Fig. 1C) and were predicted to be damaging with high confidence (Supplementary material, Table S4). Among them, Gln^{87}, homolog of Gln^{61} in RAS proteins, is directly involved in catalysis (18,19). The p.Gln87Leu substitution had previously been reported as a rare somatic event in lung carcinoma, and mutations affecting Gln^{61} are among the most recurrent oncogenic lesions in *RAS* genes (COSMIC database, http://cancer.sanger.ac.uk/cancergenome/projects/cosmic/). Likewise, p.Gly39dup altered the G1 motif participating in GTP/GDP binding and GTPase activity (Fig. 1B). Within this motif, Gly^{12} and Gly^{13} (Gly^{38} and Gly^{39} in RRAS) represent major mutation hot-spots in human cancer (COSMIC database) and account for the majority of germline *HRAS* mutations causing Costello syndrome (20). Of note, analogous insertions in RAS proteins have been reported in JMML and other malignancies (21–24). In contrast, no somatic/germline *RAS* mutation affecting Val^{29}, homolog of Val^{55} in RRAS, had previously been reported. Val^{55} side-chain is not directly involved in GTP/GDP binding, GTP hydrolysis or interaction with effectors. However, it has been reported that H-bonds are possible between the backbone of Val^{29} in HRAS and GDP/GTP (25). Furthermore, it has been suggested that Val^{29} can play a role in the transition between the GDP- and GTP-bound states (26), as supported by the evidence that the Val29Gly substitution in HRAS accelerates the GDP/GTP exchange *in vitro* (27).

Molecular dynamics (MD) simulations were performed to predict *in silico* the effects of p.Val55Met on the structure and dynamics of RRAS (Fig. 2). The mutation was introduced in the available crystallographic structure of RRAS in complex with GDP and Mg^{2+}, and the system was simulated in water for 200 ns. For comparison, MD simulations were also performed using the wild-type protein, which maintained a stable structure along the whole simulation, as expected (Fig. 2A, left panel). In contrast, a dramatic local structural transition extending up to the switch I region (residues 58–64), which mediates effector binding, was documented for the $RRAS^{V55M}$ mutant, after ~80 ns (Fig. 2A, right panel). This conformational transition resulted in an increased solvent exposure of Met^{55}, in agreement with the higher hydrophilicity of this residue compared with Val, and was accompanied by the formation of a stable

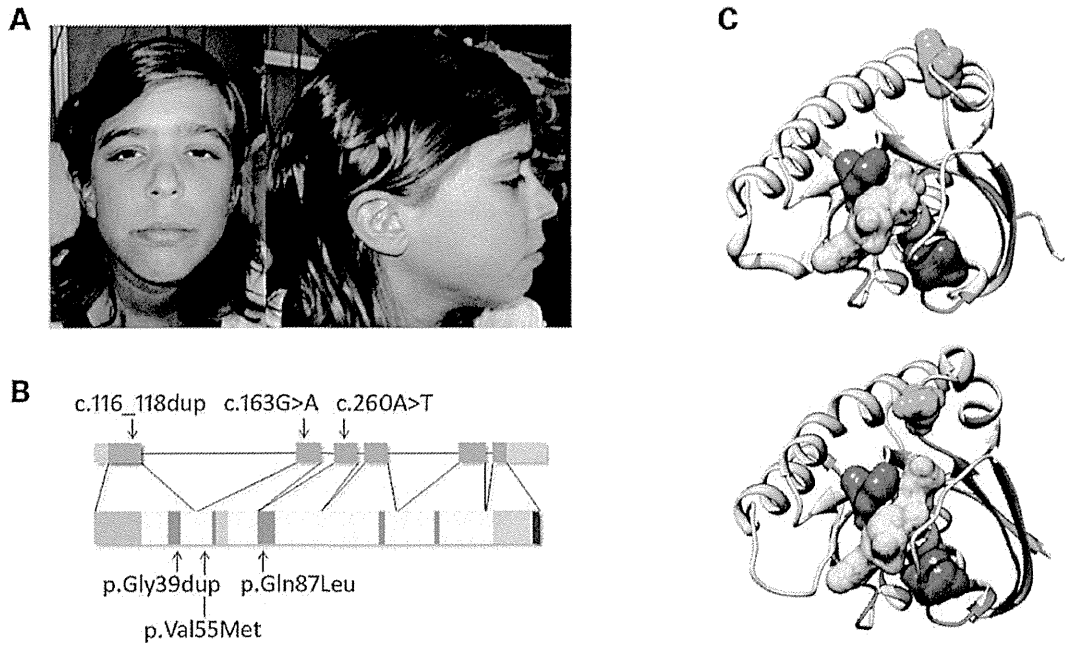

Figure 1. RASopathy-causing and leukaemia-associated *RRAS* mutations. (**A**) Facial features of the affected subject (9802) heterozygous for the *de novo* germline c.116_118dup. (**B**) *RRAS* exon–intron arrangement with coding exons as blue boxes. RRAS functional motifs include the GTP/GDP binding domain (G1 to G5, starting from the *N*-terminus) (red), switch I (light green), switch II (dark green) and hypervariable region (light brown) with the *C*-terminal CAAX motif (dark brown). The unique *N*-terminal region is also shown (violet). Location of disease-associated mutations is reported. (**C**) Position of affected residues on the three-dimensional structure of RRAS in its GDP-bound, inactive state (PDB: 2FN4) (above) and that of non-hydrolysable GTP analogue (GppNHp)-bound, active HRAS (PDB: 5P21) (below). The red surface indicates Gly^{39} and Val^{40} (Gly^{13} and Val^{14}, in HRAS), whereas Val^{55} (Val^{29}) and Gln^{87} (Gln^{61}) are shown in blue and green, respectively. GDP is reported as semi-transparent yellow surface.

cluster involving residues Ile^{50}, Met^{55} and Tyr^{58} (Fig. 2A and Supplementary material, Table S5) permitted by the unbranched and long side-chain of Met^{55}. No further significant conformational changes were observed for the remaining interval of the simulation. The major effect of this structural rearrangement was to increase exposure of GDP to the solvent (Fig. 2B), with an almost doubled solvent accessible surface area of the nucleotide after the conformational transition. This structural rearrangement was accompanied by a perturbation of the intermolecular H-bond network stabilizing GDP binding, with loss of the H-bonds between residues at codons 55 and 56, and GDP (Supplementary material, Table S5). Of note, a possible impact of the described structural transition on RRAS binding to GEF proteins, which bind to this region and mediate GDP release, was also noticed. Specifically, we observed that after the conformational rearrangement, the $RRAS^{V55M}$ region implicated in GEF binding populated a structure similar to that assumed in RAS/GEF complexes (Fig. 2C), suggesting a possible enhanced interaction of the disease-associated RRAS mutant with GEFs. In particular, Tyr^{58} was observed to adopt a side-chain orientation very similar to that of the RAS homolog Tyr^{32} in the HRAS/SOS1 complex, which has been shown to contribute to the structural rearrangements of switch I and interaction with GEFs (28–30).

Overall, these data supported an activating role of p.Val55Met through enhanced GDP release as a result of a decreased affinity for the nucleotide and/or enhanced interaction with a GEF.

Biochemical and functional characterization of RRAS mutants

Previous studies documented the gain-of-function role of p.Gln87Leu on RRAS function, and MAPK and PI3K/AKT signalling (31). To characterize the impact of p.Val55Met and p.Gly39dup on protein function, we analysed the intrinsic and GEF-accelerated nucleotide exchange reaction of these mutants. Dissociation kinetics analysis demonstrated a dramatically increased intrinsic ($RRAS^{G39dup}$) and GEF-stimulated ($RRAS^{G39dup}$ and $RRAS^{V55M}$) dissociation rate of mantGDP, indicating a facilitated nucleotide release in both mutants (Fig. 3A). RAS proteins exhibit low intrinsic GTPase activity that is enhanced by GAPs (32). Assessment of $RRAS^{G39dup}$ and $RRAS^{V55M}$ GTPase activity documented a significantly reduced intrinsic and GAP-stimulated GTP hydrolysis in the former (Fig. 3B and Supplementary material, Fig. S5). Finally, the interaction of RRAS proteins with various effectors was analysed by fluorescence polarization (Fig. 3C). While $RRAS^{WT}$ was found to bind to RAF1, RALGDS, RASSF5 and PLCE1 less efficiently than HRAS, an increased binding affinity to PIK3CA was observed. Compared with $RRAS^{WT}$, aberrant binding behaviour of the two RRAS mutants was demonstrated, with $RRAS^{G39dup}$ exhibiting an increased binding affinity towards PIK3CA, RAF1, PLCE1 and RASSF5, and $RRAS^{V55M}$ to RALGDS.

To gain further insights into the impact of disease-causing mutations on RRAS functional dysregulation and explore their effects on RAS signalling, the activation state of RRAS proteins